RSC Advances

ROYAL SOCIETY OF CHEMISTRY

www.rsc.org/advances

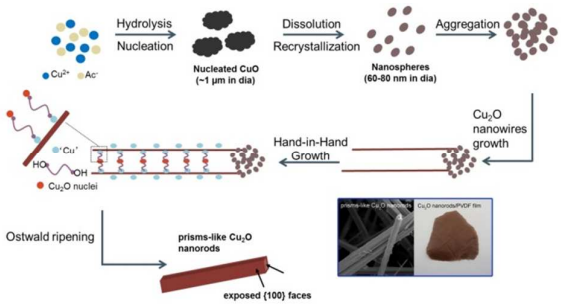

Scheme 1. Illustration of the formation of prism-like Cu_2O nanorods.

The EG acts as a "bridge" which control the "hand-in-hand" growth and makes the Cu_2O wires transform to prism-like nanorods.

RSC Advances

RSCPublishing

ARTICLE

EG-Assisted Hand-in-Hand Growth of Prism-like Cu_2O Nanorods with High Aspect Ratios and Their Thermal Conductive Performance

Cite this: DOI: 10.1039/x0xx00000x

Received 00th January 2014,
Accepted 00th January 2014

DOI: 10.1039/x0xx00000x

www.rsc.org/

Jingchao Zhu†, Yang Shang†, Xiaobo Sun* and Lin Guo*

In this work, one-dimensional, monodisperse prism-like Cu_2O nanorods with a significantly high aspect ratio (~100) have been successfully achieved by a simple hydrothermal synthesis with the assistant of ethylene glycol (EG). The nanorods, which we obtained, expose {100} faces and have a rectangular cross section. Their length, thickness and width are in the range of 50-100 μm, 0.5-1 μm and 0.5-1.5 μm respectively. Pyrrole (Py) and EG are playing important roles in the formation of the prism-like nanorods. The Py acts as a structure-directing reagent to make the Cu_2O crystal grow along [100] direction. The EG acts as a "bridge" which control the "hand-in-hand" growth of the intermediate Cu_2O nanowires and makes them to transform to the prism-like nanorods. Those products are firstly employed as a thermal conductive nanofillers to improve thermal conductivity of Poly (vinylidene fluoride) (PVDF)-based polymer composites. The original thermal conductivity studies indicate that the rod-type structural nanomaterials are very efficient fillers for polymer composites. When they were embedded in PVDF matrix with 30wt %, the Cu_2O nanorods will show a thermal conductivity enhancement (TCE) of 275% compared with the pristine PVDF. This is 1.4 times higher than the commercial Cu_2O (cubes) as fillers in PVDF composites.

Introduction

Fabrication of nano-materials has been one of the hottest branches of nanoscience due to their excellent and unique properties.[1-3] To date, the application of nano-materials has been extended to almost all conceivable fields of science and technology, ranging from daily products to aerospace materials.[4,5] Continued progress of micro/nano-size devices with increasing power density in electronic chips has required developing high-effect thermal interface materials to resolve heat removal problem.[6,7] Nanofillers are undoubtedly one of the best ways to work for the problem.[8,9] As reported, the potential nanofillers include alumina (Al_2O_3),[10] zinc oxide (ZnO),[11] aluminum nitride (AlN)[12] and silver (Ag),[13]etc. As shown in periodic table, copper and zinc is neighbor element as transition metals in the same period. Furthermore, silver and copper are at the same group. Thus, it would expect that copper and its oxide could be used as efficient fillers in thermal conductive polymer composites.

Cuprous oxide (Cu_2O), an important metal oxide with a band gap of 2.0-2.2 eV, has potential applications in many fields, such as solar cell,[14] hydrogen energy conversion,[15] catalysis,[16] gas sensor[17] and electrode materials.[18] Due to these extensive practical applications, various well-defined Cu_2O nanostructures have been synthesized in the past decades, such as nanospheres,[19] polyhedra,[20,21] and complex nanostructures.[22-24]

It is well known that, the properties of nano-materials are highly size and shape dependent.[25] Recently, a number of investigations have shown that the thermal conductivity of nano-materials based polymer composites depends on not only the sizes but also their shapes.[26] The control of shape in addition to size of fillers with high aspect ratio is of importance for thermal management applications.[27] However, there are limited papers reported on preparation of well-defined Cu_2O nanorods compared with other 1D nanostructures. Chang et al. reported the preparation of Cu_2O nanorods with a diameter of 60 nm and length of 450 nm via electro-deposition into a PAA template.[28] However, template methods always require a multi-step procedure, in addition, removal of the templates is inevitably deleterious to the pristine structure.[22] The direct synthesis of Cu_2O nanorods still remains a great challenge. Hydrothermal method is the simple and probably the most feasible method to prepare 1D nanoscale materials. As the crystal growth is anisotropic, it is prone to grow slowly toward 1D direction under the hydrothermal conditions with catalyst.[29] Therefore, it would be very interesting to synthesize Cu_2O nanorods by hydrothermal method and investigate the thermal conductivity properties of Cu_2O nanorods with high aspect ratio, which have been seldom reported.

In the present work, we synthesized prism-like Cu_2O nanorods through the reduction of ($CuAc_2$•H_2O) with Py as the reductant agent in a deionized water/EG mixed solvent under hydrothermal conditions. The as-prepared prism-like nanorods was 50-100 μm in length, 0.5-1 μm in thickness, and 0.5-1.5 μm in width. A "hand-in-hand" growth mechanism was proposed to understand the formation of prism-like structure. Moreover, the performance characteristic of the nanorods structured material as thermal conductive nanofillers was firstly presented in PVDF-based thermal composites.

Experimental

Materials

Cupric acetate ($CuAc_2$•H_2O), N,N-dimethylformamide (DMF), pyrrole (Py), commercial Copper(I) oxide (Cu_2O) cubes (diameter 2.5 μm, purity 99%) were purchased from a commercial source (Aladdin) and used as received. Poly (vinylidene fluoride) (PVDF, Mw ~ 534,000) power was obtained from Sigma-Aldrich.

The Synthesis of Cu_2O nanorods

First, $CuAc_2$•H_2O (0.16 mmol) was dissolved in a deionized water/ethylene glycol mixed solvent (43 mL H_2O + 250 μL EG), and stirred for 10 min. Then, Py (22 μL) was added to the solution and stirred for another 10 min. All the procedures were kept in a water bath at 35°C. Then the reaction mixture was transferred to a 45 mL autoclave and maintained at 140°C for 24h. After subsequently cooled to ambient temperature naturally, the red-brown sediments were formed at the bottom of the autoclave. The product was centrifuged, washed with ethanol for six times and dried at 60°C.

Preparation of PVDF/Cu_2O Composites

Firstly, the Cu_2O nanorods sample was grinded into power to make it easier dispersed in DMF. The fine powder was formed and used for subsequent fabrication. PVDF was dissolved in DMF 3 mL and stirred for 60 min to form a stable solution. Secondly, a certain amount of Cu_2O fine powder (the total amount of Cu_2O and PVDF was 300 mg) was added into the PVDF/DMF solution, and the resulting mixture was sonicated for 180 min to form a relatively stable suspension solution. Finally, a film was cast from the viscous PVDF/Cu_2O DMF solution onto a glass plate by a scraper. The film was dried in a vacuum oven at 60°C for 8 h to evaporate the solvent slowly, and the PVDF/Cu_2O composite film was obtained with 3 cm x 6 cm in size and about 20 μm in thickness.

Characterization

The structure of the products was characterized by the powder X-ray diffraction (XRD) using a RigakuRotaflexDmax2200 diffractometer with Cu Kα radiation (λ = 1.5406 Å). Scanning electron microscopy (SEM) images of the samples were obtained using Hitachi S-4800 with an accelerating voltage of 10 kV. High-resolution transmission electron microscopy (HRTEM), Transmission electron microscopy (TEM) and High-resolution transmission electron microscopy (HRTEM) images were recorded by JEOL JEM-2100F with an accelerating voltage of 200 kV. The thermal conductivity of composite film was evaluated by Hot Disk Thermal Analyzer (TPS 2500S, Sweden) equipped with a 30-mm diameter Kapton sensor disk, which setup following by the transient hot-strip method. The technique is based on recording the transient temperature increase of a 25-μm-thick, 8-mm-wide, and 70-mm-long iron strip clamped between two sample halves and heated with a constant direct current in the temperature range 20° to 700°C.

Results and discussion

Characterization of prism-like Cu_2O nanorods

The crystallographic structure of the as-prepared products was confirmed by X-ray diffraction (XRD). As shown in Fig. 2d, all the diffraction peaks (2θ = 29.7°, 36.4°, 42.3°, 61.4° and 73.5°) could be well indexed to the cubic Cu_2O (JCPDS No.05-0667). No other diffraction peaks from the possible impurities such as CuO or Cu could be identified, indicated their purity.

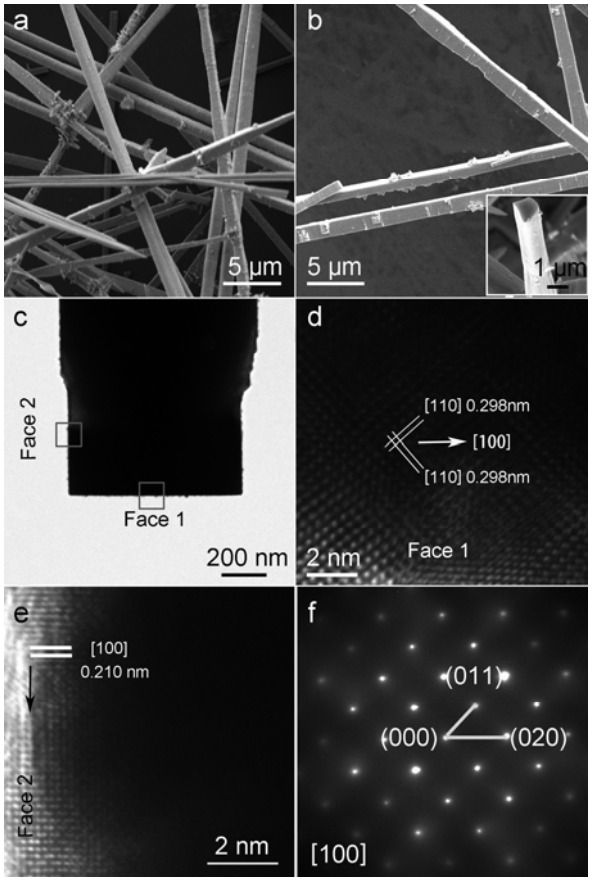

Fig. 1 (a,b)SEM images of prism-like Cu_2O nanorods with different magnifications. Inset of (b) SEM image of the cross section of an individual nanorod. (c) TEM image of the end of an individual nanorod. (d) HRTEM image of the bottom frame area in (c). (e) TEM image of the left frame area in (c). (f) Corresponding SAED pattern viewed along the [100] directions of the individual nanorod as in (c).

Top-view scanning electron microscopy (SEM) image (Fig. 1a) indicated that the as-prepared products were a mass of straight prism-like nanorods and were quite uniform in size. The average size of the nanorods was measured as 50-100 μm in length, 0.5-1 μm in thickness, and 0.5-1.5 μm in width. Thus, the aspect ratio of the Cu_2O nanorods was on the order of 50-100. Zooming on an individual nanorod (Fig. 1b), it could be seen that the surface of the nanorod was not completely smooth but with some small bumps. Interestingly, unlike other nanorods, the cross section of the nanorods was rectangular rather than round (inset in Fig. 1b). The detailed structure and the growth direction of the nanorods were examined by transmission electron microscopy (TEM) and selected-area electron diffraction (SAED) analysis. Fig. 1c recorded at the end of an individual nanorod highlighted the rectangular feature of cross section. The measured two vertical sets of lattice fringes in the high-resolution transmission electron microscopy (HRTEM) image (the bottom frame area in Fig. 1c) was *ca.* 0.298 nm, coincident well with the (110) crystal plane of the cubic Cu_2O, demonstrating that the Face 2 in Fig. 1c were {100} faces. Fig. 1e recorded at the left frame area, shown the distance between the fringes perpendicular to the wall was *ca.* 0.210 nm, that is also coincident well with the (100) crystal plane of the cubic Cu_2O, demonstrating that the Face 1 in Fig. 1c were also {100} faces. Therefore, the exposed faces of the prism-like nanorods were {100} faces. The SEAD pattern of the Cu_2O nanorods (Fig. 1f) exhibited as bright diffraction spots, revealing their single crystalline structure nature and indicating that the Cu_2O nanorods grow along the [100] direction.

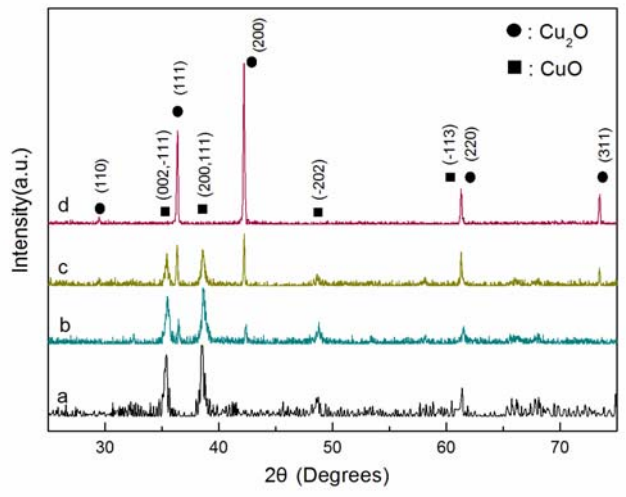

Fig. 2 XRD patterns of the intermediate products collect at (a) 2, (b) 5, (c) 8, (d) 24 h.

To understand the formation mechanism of the prism-like Cu_2O nanorods, we performed XRD characterizations and extensive electron microscopy investigation on the samples collected at different stages. After 2h, microsphereswith average sizes of 1μmwere donimated the products(Fig. 3a). The corresponding XRD pattern (Fig. 2a) of the black products consisted of four peaks at 2θ = 35.3°, 38.5°, 48.8° and 61.4°, which could be perfectly indexed to the monoclinic CuO (JCPDS No.05-0661). No other peaks from impurities such as Cu_2O can be identified. It suggest that CuO microspheres formed at the initial stage. With the reaction proceeded for 5 h, those CuO microspheres dissolved to form CuO nanospheres with diameter in range of 60-80 nm (Fig. 3b), and the corresponding HRTEM image (Fig. 3e recorded at the black frame area in Fig. 3b) verified that the distant between the fringes was *ca.* 0.253 nm, which corresponded to the the spacing between (002) lattice plane of CuO. Besides the CuO nanospheres, nanowires with diameter in range of 250-300 nmappeared(Fig. 3b). HRTEM image of the nanowire (Fig. 3f recorded at the white frame area in Fig. 3b) shown that the distant between the fringes was *ca.* 0.295 nm, which corresponded to the spacing between (110) lattice plane of Cu_2O.The corresponding XRD pattern (Fig. 2b) also demonstrated the formation of Cu_2O that besides the greatly reducing diffraction peaks from CuO,

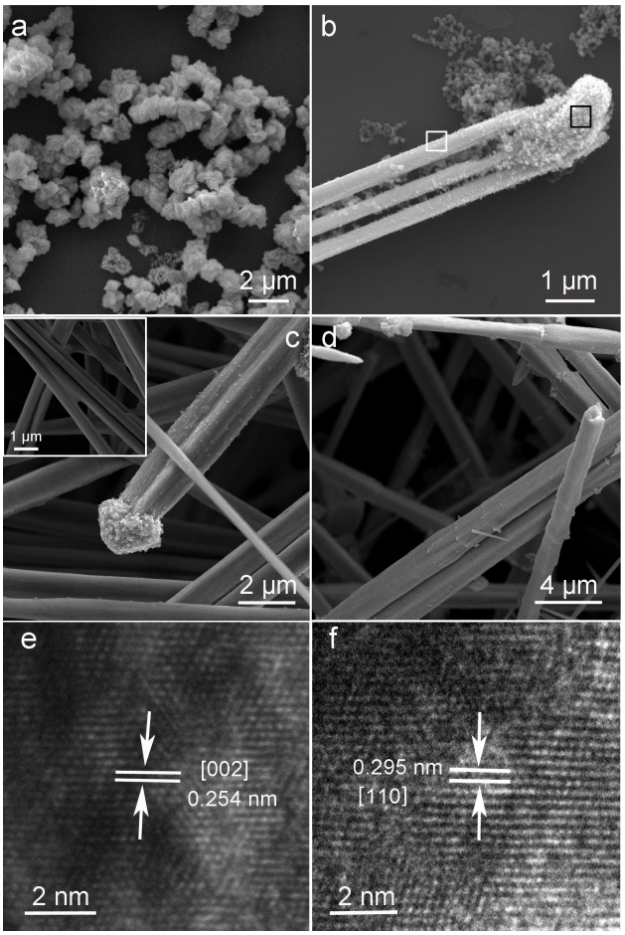

Fig. 3SEM images of the intermediate products collect at (a) 2, (b) 5, (c) 8, (d) 24 h. (e) TEM image of the black frame area in (b). (f) TEM image of the white frame area in (b).

two new peaks emerging at 2θ = 36.4° and 42.3°, which agree well with the cubic Cu_2O (JCPDS No.05-0667). When the reaction reached to 8 h, the amount of CuO nanospheres significantly reduced, and the products mainly consisted of Cu_2O nanowires(Fig. 3c). The greatlyintensified signals from Cu_2O in the XRD pattern (Fig. 2c) proved that Cu_2O were generated in a large number. Remarkably, those Cu_2O nanowires began to grow into nearly orderly prism-like

wire bundles, which revealed a tendency transform into prism-like nanorods. Inset of Fig. 3c clearly shown thejoint between two Cu_2O nanowires. The intermediate products obtained at 12 and 16 h clearly shown that the growth process from nanowires to nanorods (Fig. S1). It should be pointed out that, as shown in the white frame area of Fig. S1b, there were still some nanowires, this suggested that in the process of the nanowires formed into nanorods, there were still generatednew nanowires. Finally, with the hydrothermal treatment proceeded for 24 h, perfect prism-like Cu_2O nanorods formed (Fig. 3d). The corresponding XRD pattern (Fig. 2d) demonstrated that the diffraction peaks from Cu_2O dominated the while those from CuO disappeared. The obtained products were still prism-like Cu_2O nanorods if further extend the reaction time to 48 h (Fig. S2).

Combined the composition and the structure characterization, the growth process of prism-like Cu_2O nanorods can be divided into three stages. In the initial stage, uniform CuO microspheres formed through a two-step reaction process as shown below:

$$Cu^{2+} + H_2O \rightarrow Cu(OH)_2 + 2H^+$$

$$Cu(OH)_2 = CuO + H_2O$$

Li et al. reported[30] that the organic monomer, such as Py, could act as a reductant agent during the hydrothermal process. However, due to the weak oxidizing ability of the Cu^{2+}, the reduction process for Py reduce $Cu^{2+}$to Cu^+ should be carried out at temperature above 110°C under hydrothermal conditions. In our case, the temperature inside the autoclave may not high enough to reduce Cu^{2+} to Cu^+ by Py within 2 h. Thus, only CuO formed, and aggregated as spherical shape to lower the surface energy. In addition, it is well-known that Py can also act as a structure-directing reagent to make the crystal grow along a particular direction[32]. Because of the rapid aggregation process of CuO, the role of Py for structure directing agent did not work.

In the next stage, as the reaction proceed for 5 h, with the temperature and pressure inside the autoclave further increased, the redox reactions between Py and CuO could occur, subsequently, CuO microspheres gradually decomposed to CuO nanospheres with diameter in range of 60-80 nm **(**Fig. 2b**)**[31]. Meanwhile, due to the slow reduction process, Py would act as the structure-directing reagent to induce the growth of nanowires (Fig. 2b). To confirm the role of Py, control experiment was carried out by removing the Py while kept other conditions unchanged (with only EG in the reaction solution). As shown in Fig. S3b, only black products (CuO) with irregular spheres-like morphology obtained.To further investigate the effect of EG,experiments were carried out without EG and Py in the reaction solution. The obtained product was still black (CuO) with irregular spheres-like morphology (Fig. S3a). It suggested that the addition of EG didn't have a significant effect on the formation of nanospheres.

In the last stage, with the Cu_2O nanowires formed in a large number, EG began to play an important role in the formation of prism-like Cu_2O nanorods. Control experiments demonstrated that only Cu_2O nanowires obtained without EG. By contrast, when EG was introduced, the Cu_2O nanowires could grow into prism-like nanorods. In addition, the prism-like nanorods became increasingly apparent with theincrease of EG. (Fig. S4) As reported before,[36] EG could play a major role in the hydrothermal process as co-surfactant in an aqueous system. EG has two hydroxyl groups (-OH) at both ends, when it was introduced to the reaction solution, one end of the negative charge 'OH' group could interact with the positively charged 'Cu' on the surface of Cu_2O nanowires.[37] And the other 'OH' group of EG could interact with the later formed Cu_2O nuclei from the reaction solution. Thus, we speculated that the EG may act as a "bridge" and control the Cu_2O nanowires grow "hand-in-hand" into prism-like Cu_2O wire bundles. Following the Ostwald ripening process, the Cu_2O wire bundles gradually transformed into prism-like Cu_2O nanorods with exposed {100} faces, it is consisted with the equilibrium form of a crystal tends to possess a minimal total surface energy.

We further investigate effect of temperature on the final products. When the reaction temperature decreased to from 140℃to 120℃, the product mainly consisted of microspheres with average sizes about 1-2 μm. Besides the microspheres, there was a small quantity of irregular nanorods structure. When the reaction temperature increased to 160℃ (as shown in Fig S5b), the Cu_2O nanorods assembled to hierarchical structures. Only when the reaction temperature was 140℃ could get the prism-like Cu_2O nanorods.

Based on the above analysis, we speculate that the formation of the prism-like Cu_2O nanorods occurred through a "hand-in-hand" growth process and the probable growth route is illustrated in Scheme 1.

Thermal properties of the Cu_2O/PVDF composite

PVDF was selected as the matrix due to its good thermal stability and easily processing. The thermal conductive PVDF/Cu_2O composites films were typically prepared by using solvent assistant mixing. The Cu_2O nanorods fine powder was added into the PVDF/DMF solutions, followed by 180 min water sonication to reach a relatively stable suspension solution. The PVDF/Cu_2O composite film was obtained with composite loading in the range of 10-30 wt %. The through-plane conductivity of the composite was measured with hot disk thermal analyzer, which operated on the transient hot-strip method. In this technique, the bulk through-plane thermal conductivity is calculated from the slop of the temperature versus time. [38]

The thermal conductivities of the Cu_2O/PVDF composites are shown in Fig. 4. The room temperature thermal conductivity of the pure PVDF is about 0.12 W/mK. Whatever Cu_2O nanorods or commercial Cu_2O cubes are used as fillers, the Cu_2O/PVDF composites reveal dramatic enhancement of thermal conductivity in comparison with the pure PVDF. When commercial Cu_2O cubes are used as fillers, thermal conductivities of PVDF-based composites are given a slight increase, and show linear relationship versus loading as shown in Fig. 4 (round line). However, for the prism-like Cu_2O nanorods, it should be noted that the improvement of thermal conductivity in the Cu_2O/PVDF nanocomposites is nonlinear (See Fig. 4 square line). At low loading (below 10 wt%), Cu_2O nanofillers dispersed randomly in the PVDF matrix result in the slight increase for thermal conductivity. At high filler loading, the thermal conductivity increased evidently with increasing Cu_2O content. When 30 wt% loading of the Cu_2O nanorods embedded in

RSC Advances RSCPublishing

ARTICLE

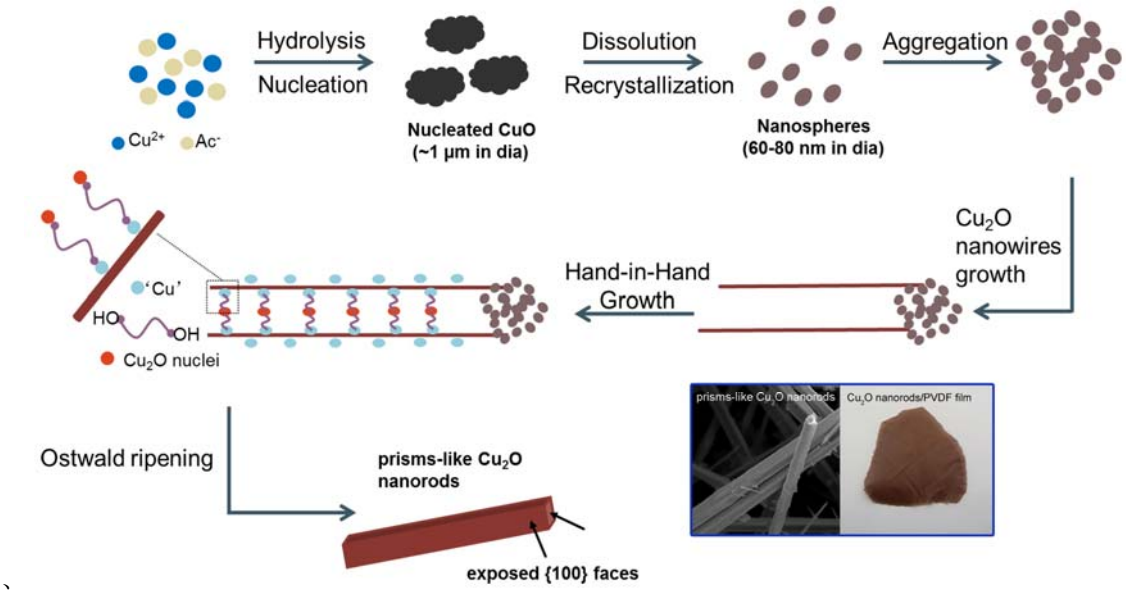

Scheme 1. Illustration of the formation of prism-like Cu_2O nanorods.

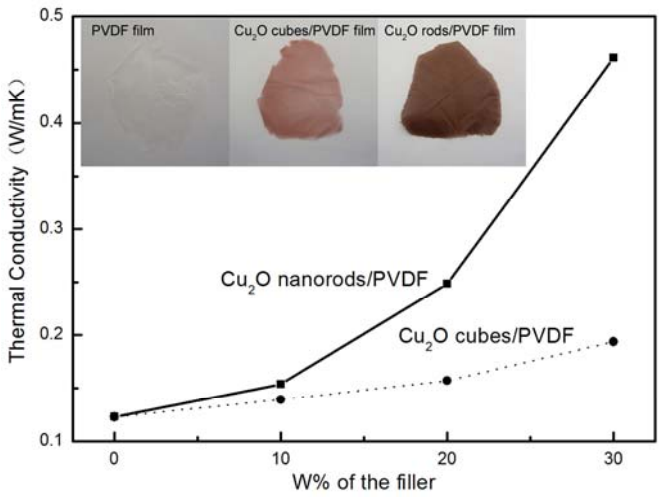

Fig. 4 Thermal conductivities of Cu_2O/PVDF composites as a function of weight fraction for Cu_2O nanorods and Cu_2O cubes.

PVDF matrix, thermal conductivity of composites is 2.7 times higher than that of pristine PVDF.

This implies that efficient thermal transfer pathways start to form at a high fraction of nanorods due to rod-to-rod connection networks. It is believed that at a Cu_2O nanorods fraction of higher than 30 wt%, a more effective improvement is expected: Fig. 5 shows the thermal conductivity enhancement (TCE, κ-κ_0/κ) versus weight loading for PVDF composites with commercial Cu_2O cubes and prism-like Cu_2O nanorods fillers. The thermal conductive performance of Cu_2O nanorods/PVDF composites is much better than that of Cu_2O cubes/PVDF composites. At 30 wt% fillers loading, the TCE value of Cu_2O nanorods-based composites is in the order of 5 times more than those of Cu_2O cubes. The obvious difference between these two fillers is aspect ratio of particles. As recently reported, the control of shape in addition to size of fillers with high aspect ratio is of significant importance for thermal property improvement. These comparative results clearly confirm the improvement of thermal conductivity performance of composites with aspect ratio increasing. As shown in Fig. 1, the Cu_2O nanorods have a high aspect ratio and perfect prism-like nanostructure, but commercial Cu_2O cubes are polyhedral in size of about 2.5 μm (Fig. S6). After calculation, the aspect ratio of the Cu_2O nanorods is on the order of 50-100, which approach to the aspect ratio of the highest effect filler SWCNTs (100~1000). The contribution on the thermal conductivity of the Cu_2O fillers increases as the aspect ratio increasing, which is apparently responsible for the improved thermal performance of the Cu_2O in comparison with previous measurements on similar fillers.

In comparison with the researches that have been carried out on the thermal conductivity of the inorganic/ceramic polymer composites, not much work has been done on 1D nanofillers-based polymer composite. Most of them are studied on nanoparticles, such as AlN nanoparticles could give a TCE value 87 % with 27.5 wt%

loading of fillers in epoxy composites,[39] and Al_2O_3 nanofillers reach 60 % TCE with 30 wt% loading in PVDF composites.[40]The Cu_2O cubes in this study can reach the same level for thermal improvement with same filler loading. Among the few work on 1D inorganic nanofillers, only nanowire and nanotube have been reported, such as ZnO nanowire and boron nitride nanotube (BNNT).

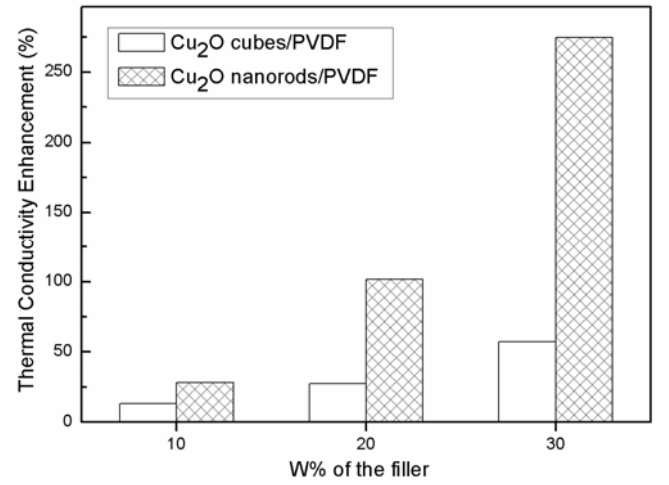

Fig. 5 Thermal conductivity enhancement comparison for Cu_2O nanorods and Cu_2O cubes in PVDF matrix at different fillers loading.

To our acknowledgement, there are still no thermal studies done on the inorganic nanorods structure. The performance of Cu_2O nanorods based composites is approached to that of ZnO nanowire published.[38] In the case of BNNT, it gives a much better thermal conductive performance due to its high intrinsic thermal conductivity with very low dielectric constants.[9] However, BNNT is always synthesized with CVD, and hard to scale synthesis with simple method. Further enhancement in thermal conductivity of Cu_2O nanorods-based composite may be possible if the dielectric constants could be reduces. This might be achieved by introducing physical or chemical functionalities on the surface of the Cu_2O nanorods as worked for AlN and BNNT-based composites.[9,12,] Therefore, these initial results and advantage of Cu_2O nanorods will render Cu_2O-based composites as potentially thermally conductive material for application in electronic devices.

Conclusions

In conclusion, we have successfully suggested an effective hydrothermal treatment method to prepare prism-like 1D Cu_2O nanorods with high aspect ratio (~100). The "hand-in-hand" growth mechanism was proposed in the present work. The EG acts as a "bridge" which controls the "hand-in-hand" growth of the intermediate Cu_2O nanowires, and makes them to transform to the prism-like nanorods. When embedded in PVDF matrix, the prism-like Cu_2O nanorods shows a larger thermal conductivity enhancement compared with that of pristine PVDF. The significant suppression of thermal conductivity of the 1D nanofillers-based composites is attributed possibly to the presence of rod-to-rod connection networks. Further work on increasing fillers loading or/and decreasing dielectric constants of nanorods by chemical functionalization will be convinced to improve thermal performance of the composites. We therefore demonstrate a rod-type material structure for the development of thermal interface materials.

Acknowledgements

The project is supported by the National Key Basic Research Program of China (2010CB934700), National Natural Science Foundation of China (51272012), Innovation Foundation of BUAA for PhD Graduates and Fundamental Research Funds for the Central Universities.

Notes and references

*Corresponding authors
†These authors contributed equally to this work
School of Chemistry and Environment, Beihang University, Beijing 100191, PR China
E-mail: guolin@buaa.edu.cn, sunxb@buaa.edu.cn
† Electronic Supplementary Information (ESI) available. See DOI: 10.1039/b000000x/

1 Y. Zha, H. D. Thaker, R. R. Maddikeri, S. P. Gido, M. T. Tuominen and G. N. Tew, *J. Am. Chem. Soc.*, 2012, **134**, 14534.
2 J. Qiu, Y. C. Wu, Y. C. Wang, M. H. Engelhard, L. McElwee-White and W. D. Wei. *J. Am. Chem. Soc.*, 2013, **135**, 38.
3 M. C. Orilall and U. Wiesner, *Chem. Soc. Rev.*, 2011, **40**, 520.
4 M. H. Huang and P. H. Lin. *Adv. Funct. Mater.*, 2012, **22**, 14.
5 J. C. Pang, G. H. Fan, X. P. Cui, A. B. Li, L. Geng, Z. Z. Zheng and Q. W. Wang, *Mat. Sci. Eng. A-Struct.*, 2013, **582**, 294.
6 P. Zhang, Q. Li and Y. Xuan, *Compos. Part. A-Appl. S.*, 2014, **57**, 1.
7 Y. J. Heo, H. T. Kim, K. J. Kim, S. Nahm, Y. J. Yoon and J. Kim, *Appl. Therm. Eng.* , 2013, **50**, 799.
8 X. Sun, A. Yu, P. Ramesh, E. Bekyarova, M. E. Itkis and R. C. Haddon, *J. Electron. Packag.*, 2011, **133**, 020905.
9 X. Huang, C. Zhi, P. Jiang, D. Golberg, Y. Bando and T. Tanaka, *Adv. Funct. Mater.*, 2013, **23**, 1824.
10 J. Hostaša, W. Pabst, J. Matějíček and D. J. Green, *J. Am. Ceram. Soc.*, 2011, **94**, 4404.
11 J. W. Jiang, H. S. Park and T. Rabczuk, *Nanoscale*, 2013, **5**, 11035.
12 X. Huang, T. Iizuka, P. Jiang, Y. Ohki and T.Tanaka, *J. Phys. Chem. C*, 2012, **116**, 13629.
13 V. H. Luan, H. N. Tien, T. V. Cuong, B. S. Kong, J. S. Chung, E. J. Kim and S. H. Hur, *J. Mater. Chem.*, 2012, **22**, 8649.
14 J. Xie, C. Guo and C. M. Li, *Phys. Chem. Chem. Phys.*, 2013, **15**, 15905.
15 P. D. Tran, S. K. Batabyal, S. S. Pramana, J. Barber, L. H. Wong and S. C. Loo, *Nanoscale*, 2012, **4**, 3875.
16 T. Jiang, T. Xie, L. Chen, Z. Fu and D. Wang, *Nanoscale*, 2013, **5**, 2938.
17 L. Guan, H. Pang, J. Wang, Q. Lu, J. Yin and F. Gao, *Chem. Commun*, 2010, **46**, 7022.
18 L. Hu, Y. Huang, F. Zhang and Q. Chen, *Nanoscale*, 2013, **5**, 4186.
19 Y. Shang, D. Zhang and L. Guo. *J. Mater. Chem.*, 2012, **22**, 856.
20 W. C. Huang, L. M. Lyu, Y. C. Yang and M. H. Huang, *J. Am. Chem. Soc.*, 2012, **134**, 1261.

21 M. Leng, M. Liu, Y. Zhang, Z. Wang, C. Yu, X. Yang, H. Zhang and C. Wang, *J. Am. Chem. Soc.*, 2010, **132**. 17084.
22 J. Li, X. Huang and Y. Tan, *Nano. Res.*, 2011, **4**, 448.
23 S. Deng, V. Tjoa, H. M. Fan, H. R. Tan, D. C. Sayle, M. Olivo, S. Mhaisalkar, J. Wei and C. H. Sow, *J. Am. Chem. Soc.*, 2012, **134**, 4905.
24 P. Lignier, R. Bellabarba and R. P. Tooze, *Chem. Soc. Rev.*, 2012, **41**, 1708.
25 Y. H. Choi, D. H. Kim, H. S. Han, S. Shin, S. H. Hong and K. S. Hong, *Langmuir*, 2014, **30**, 700.
26 W. L. Song, P. Wang, L. Cao, A. Anderson, M. J. Meziani, A. J. Farr and Y. P. Sun, *Angew. Chem. Int. Ed. Engl.*, 2012, **51**, 6498.
27 A. Yu, M. E. Itkis, E. Bekyarova and R. C. Haddon, *J. Phys. Chem. C,* 2007, **111**, 7565.
28 Y. H. Lee, I. C. Leu, C. L. Liao, S. T. Chang, M. T. Wu, J. H. Yen and K. Z. Fung, *Electrochem. Solid. ST.*, 2006, **9**, A207.
29 A. A. Vargeese and K. Muralidharan, *Appl. Catal., A*, 2012, **171**, 447.
30 X. Yi, W. Tian, Q. Peng, H. Zhao, T. Wang and Y. Li. *Nano Lett.*, 2007, **7**, 3723.
31 K. Xiong, G. C. Xi, Q. B. Zhao, R. Zhang, H. B. Zhang and Y. T. Qian, *Crystal Growth & Design,*, 2006, **6**, 577.
32 N. Wang, X. Cao, Q. Chen and L. Guo, *Chem. Eur. J.*, 2012, **18**, 6049.
33 R. Zana, *Adv. Colloid Interfac.*, 1995, **57**, 1.
34 D. F. Zhang, H. Zhang, L. Guo, K. Zheng, X. D. Han and Z. Zhang, *J. Mater. Chem.*, 2009, **19**, 5220.
35 T. Log, *J. Am. Ceram. Soc.*, 1991, **74**, 941.
36 W. Peng, X. Huang, J. Yu, P. Jiang and W. Liu, *Compos. Part. A-Appl. S.*, 2010, **41**, 1201.
37 R. Qian, J. Yu, C. Wu, X. Zhai and P. Jiang, *RSC Advances*, 2013, **3**, 17373.
38 K. T. Igamberdiev, S. U. Yuldashev, H. D. Cho, T. W. Kang, S. M. Rakhimova and T. K. Akhmedov, *J. Korean. Phys. Soc.*, 2012, **60**, 1513.